Electronic Supplementary Information for

Nitrogen-doped Porous Carbon with Complicated Architecture and Superior K^+ Storage Performance

Yongsheng Zhou[a,b], Yingchun Zhu*[b,e], Bingshe Xu*[c], and Xueji Zhang*[d]*

[a] College of Chemistry and Materials Engineering, Anhui Science and Technology University, Bengbu, 233030, P. R. China

[b] Key Laboratory of Inorganic Coating Materials CAS, Shanghai Institute of Ceramics, Chinese Academy of Sciences, Shanghai, 200050, P. R. China

[c] Key Laboratory of Interface Science and Engineering in Advanced Materials, Ministry of Education, Taiyuan University of Technology, Taiyuan, 030024, P. R. China

[d] School of Biomedical Engineering, Shenzhen University Health Science Center, Shenzhen, Guangdong 518060, P. R. China

[e] Center of Materials Science and Optoelectronics Engineering，University of Chinese Academy of Sciences, Beijing 100049, P. R. China

E-mail: yszhou1981@gmail.com; zhangxueji@szu.edu.cn

Experimental section

Synthesis of N-doped carbon hollow turbostratic tube (CHTT-N) and carbon hollow turbostratic tube (CHTT)

The preparation process of nitrogen-doped nanofiber hybrid membranes is illustrated in Figure 2A. The polyacrylonitrile (PAN) nanofiber membrane was first prepared through a facile single-nozzle electrospinning technique using a commercial electrospinning system (UCALERY Beijing Co., Ltd, China). Typically, 0.5 g of PAN and 0.25 g of urea were dissolved in 4.25 g of dimethylformamide (DMF) at room temperature under magnetic stirring to form a polymer solution after stirring for 3 h to ensure complete solubility. A 4.0 g amount of $Ni(Ac)_2$ (Ac = acetate) and magnesium nitrate hexahydrate was added to the mixture, and stirring was continued until the polymer solution became clear and then loaded into a 5 mL plastic syringe. The electrospinning process was carried out at a high voltage of 20 kV at a feeding rate of 0.1 mm min^{-1} through a stainless-steel needle, which had an inner diameter of 0.5 mm. After evaporation of the solvents from the jet stream, the composite nanofibers of PAN/$Ni(Ac)_2$/$Mg(NO_3)_2$ were produced and the resulting nonwoven fiber mat was collected. All electrospinning experiments were performed at room temperature. The obtained nonwoven fiber mat was stabilized in air at 275 °C for 2 h with a heating rate of 1 °C/min.

Then, the preoxidized process of the generated PAN/$Ni(Ac)_2$/$Mg(NO_3)_2$ nanofiber membrane was generated at 180 °C in air atmosphere for 1 h with a heating rate of 1 °C min^{-1}. CHTT-N was grown on the resulting product at 1,000 °C under a gas mixture (H_2: Ar: NH_3=20: 300: 100 sccm) flow in an induction furnace. The CHTT-N was harvested after the acidic etching of the sample

by a HCl solution to remove MgO. The CHTT material was prepared in a way similar to that for the CHTT material, but NH_3 was not added to the reaction.

In addition, pure CNF was obtained by a direct preoxidization and carbonization processes of the electrospun PAN nanofiber membrane.

Characterization of materials

Scanning electron microscope (SEM) images were obtained using an S-4800 field emission scanning electron microscope (Hitachi, Japan) operating at 10 kV. The transmission electron microscope (TEM) images were obtained using a FEI Titan G_2 60-300 operating at 80 kV. X-ray powder diffraction (XRD) pattern of the sample was recorded using a D/max-3C diffractometer equipped with Cu-Kα X-ray source. Raman spectra were recorded with a Renishaw RM-1000 Micro Raman Spectrometer. Investigations of chemical compositions were performed using X-ray photoelectron spectroscopy (XPS, Physical Electronics PHI 5600). N_2 sorption analysis was conducted on an ASAP2020 accelerated surface area and porosimetry instrument (Micromeritics), equipped with automated surface area, at 77 K using BarrettEmmettTeller (BET) calculations for the surface area. The pore size distribution (PSD) plot was recorded from the adsorption branch of the isotherm based on the Barrett−Joyner−Halenda (BJH) method.

Electrochemical measurements

The electrochemical performance of as-prepared composites was carried out via CR2025 coin-type cells. The working electrodes were consisted with 80 wt% active materials, 10 wt% ketjen black, and 10 wt% carboxymethyl cellulose, which were mixed with appropriate de-ionized water, pasted on Ni foam, and dried at 80 ^oC under vacuum for 12 h. The loading density, diameter, and thickness of the prepared electrodes were ~1mg cm^{-2}, ~12 mm, and ~65 to 85 μm, respectively.

For PIBs, the counter electrode was potassium foil, and the electrolyte was 1 M KPF_6 in EC: propylene carbonate (PC) (1: 1 in volume). A glass fiber membrane (Whatman, GF/D) was used as the separator for PIBs. The galvanostatic discharge/charge test was performed on a battery tester (Land 2001A system) between 0.05 and 2.8 V under various current densities from 0.1 to 20 A g^{-1}. Cyclic voltammetry (CV) was measured on a CHI660C electrochemical workstation from 0.2 to 2.0 mV s^{-1}.

The CHTT-N//CHTT-N PIHC devices were assembled by employing the prepotassiation CHTT-N anode and raw CHTT-N cathode with a mass ratio ranging from 1:0.5 to 1:2. The mass loading of active material in the anode is ~2 mg cm^{-2}. During the prepotassiation process, the half-cell was charged−discharged for six cycles at 0.05 A g^{-1}. The electrochemical performance tests including galvanostatic charge−discharge and CV were conducted using a Gamry Interface 1000 electrochemical workstation. The power density (P, W kg^{-1}) and energy density (E, Wh kg^{-1}) of the CHTT-N//CHTT-N PIHC devices were calculated based on the total mass of anode and cathode electrodes using the following equations:

$$p = \frac{\Delta V \times I}{2\mathrm{m}} \times 1000 \quad (1)$$

$$E = \frac{P \times I}{3600} \quad (2)$$

Where Δ V (V) is the discharge voltage excluding the IR drop, I (A) is the discharge current, m (g) is the total mass of active materials, including anode and cathode, and t (s) is the discharge time, respectively.

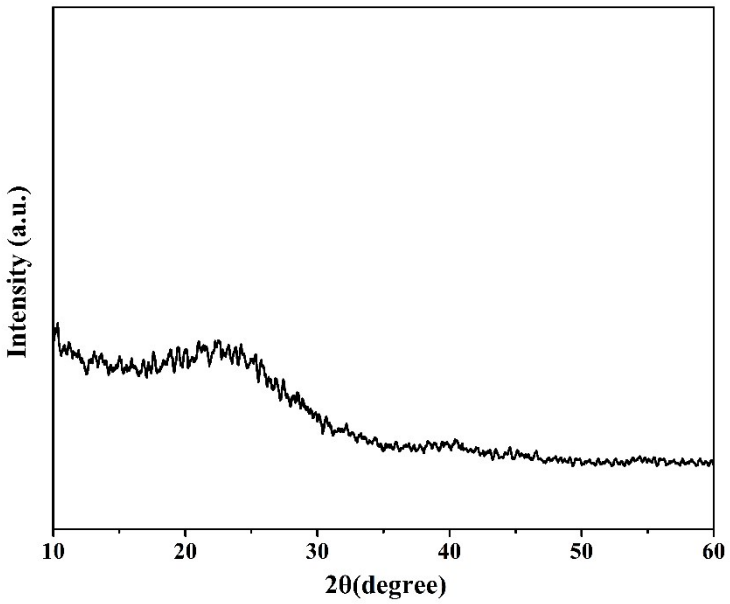

Figure S1. XRD pattern of the CHTT-N.

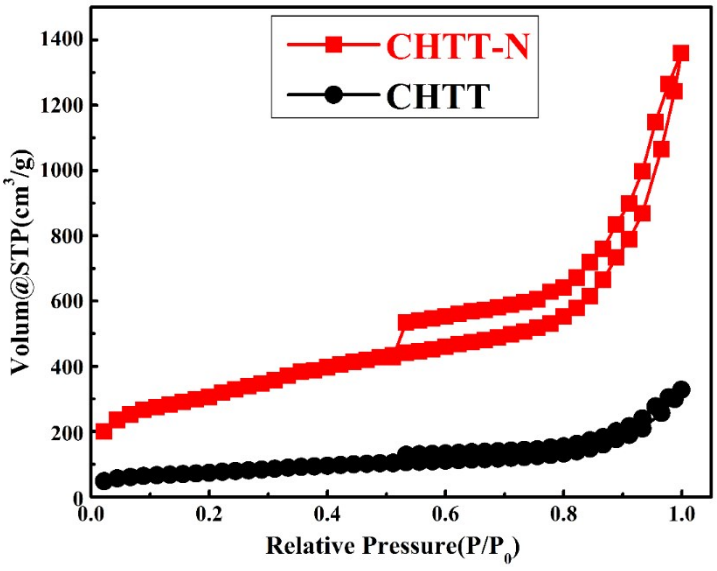

Figure S2. N_2 adsorption−desorption isotherms.

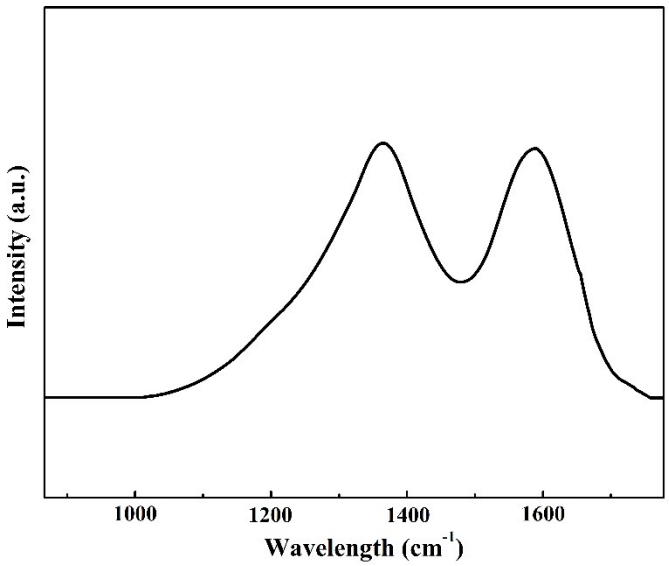

Figure S3. Raman spectra of CHTT-N.

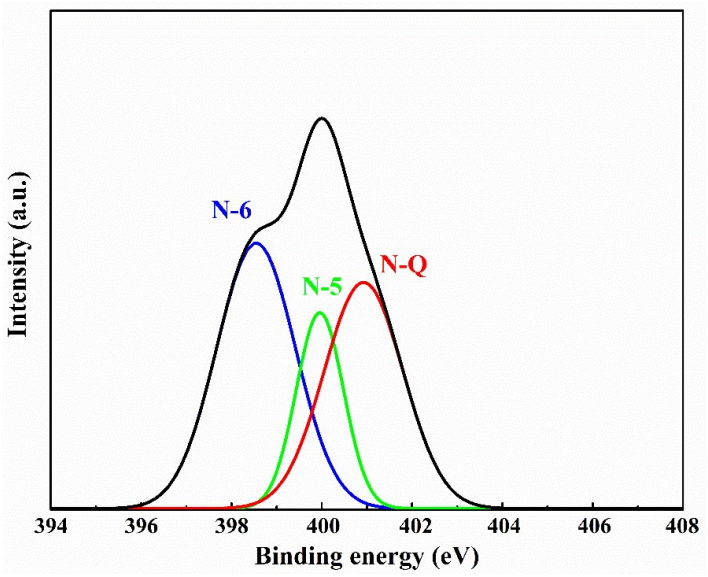

Figure S4. The fine-scanned N 1s spectra of CHTT-N.

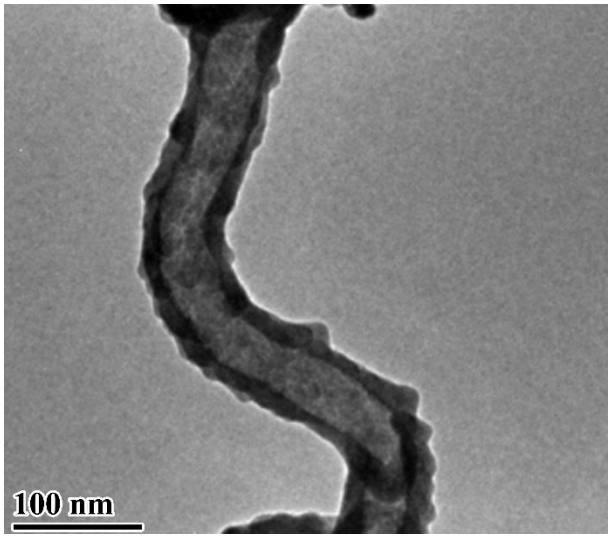

Figure S5. High-magnification TEM image of CHTT-N after 200th cycles.

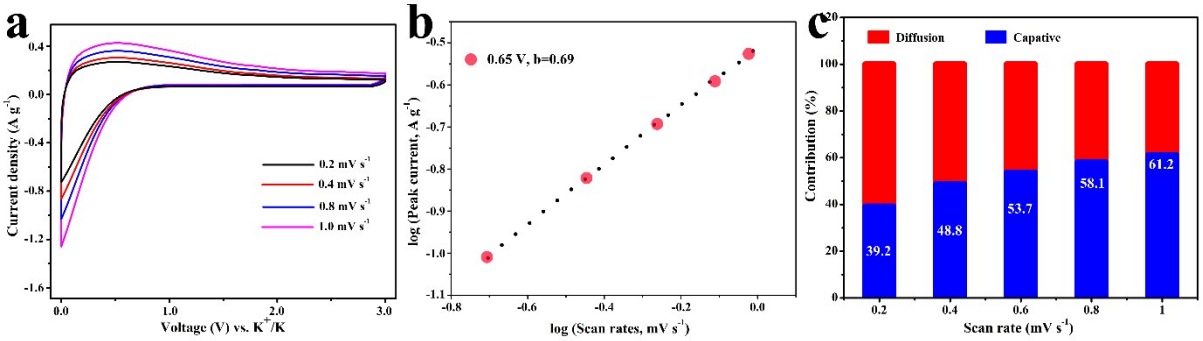

Figure S6. (a) CV curves at different scan rates from 0.2 to 1.0 mV s^{-1}. (b) Determination of the b-value according to the relationship between the peak current and the scan rate. (c) Normalized contribution proportions of capacitance and diffusion at different scan rates.

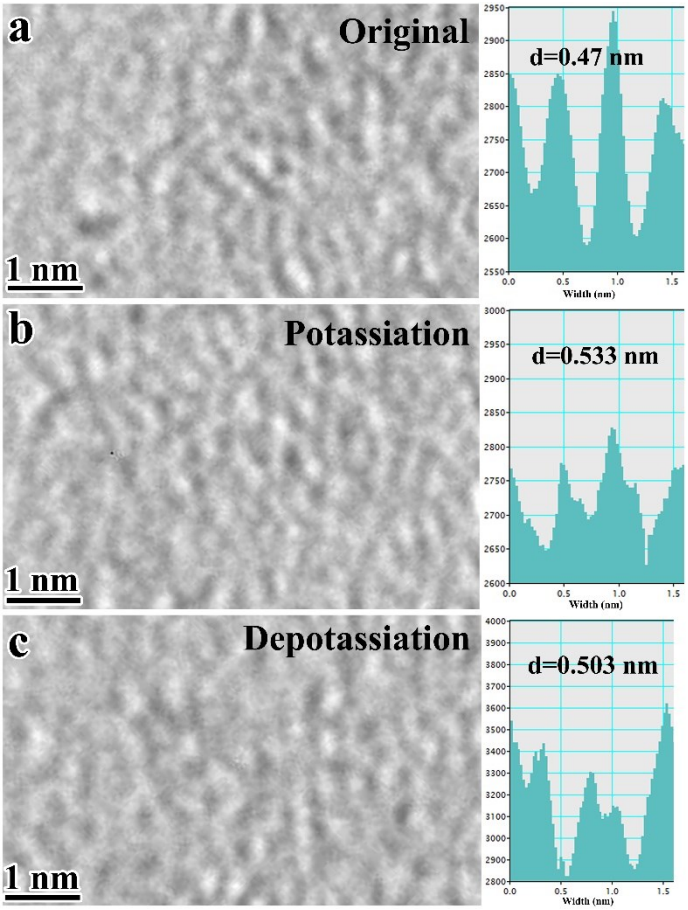

Figure S7. HRTEM images and corresponding interlayer spacing of the (a) original, (b) potassiated and (c) depotassiated CHTT-N.

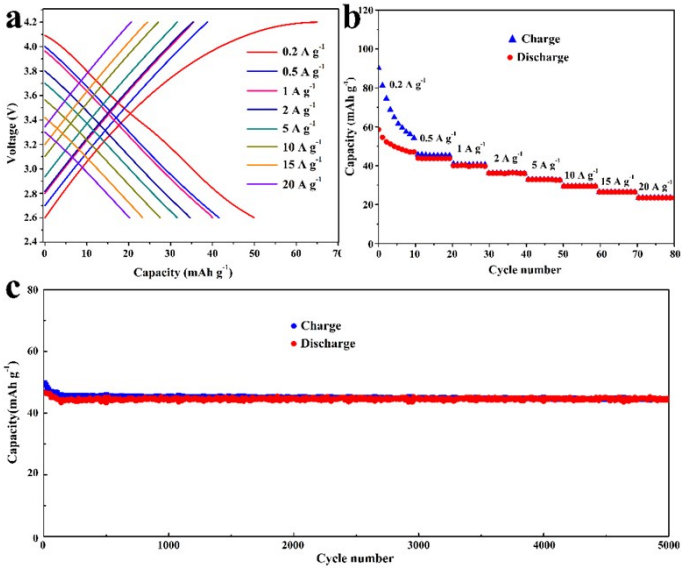

Figure S8. Electrochemical properties of the CHTT-N tested as KIB cathode. (a) charge-discharge curves, and (b) rate capability profiles at different current densities from 0.2 to 20 A g^{-1}. (c) cycle performance at current density of 2 A g^{-1} for 5000 cycles.

The electrochemical performance of CHTT-N cathodes was evaluated by using galvanostatic charge-discharge operated at high potentials of 2.5-4.2 V vs. K/K^+. As shown in Figure S6a, the charge-discharge curves of the CHTT-N materials at different current densities are highly symmetrical and quasitriangular without obvious redox peaks, which indicated that CHTT-N electrode possesses a typical capacitive behavior as desirable capacitor-type cathode material. Moreover, the CHTT-N exhibit high capacity and good rate capability at high currents (Figure S6b). The charge capacity of CHTT-N is 53.6 mAh g^{-1} at current density of 0.2 A g^{-1}. Even at a very high current density of 20 A g^{-1}, the CHTT-N cathode can still be charged to 23.5 mAh g^{-1}. The CHTT-N cathode also shows a stable cycling performance of 44 mAh g^{-1} after 5000 cycles under the current density of 2 A g^{-1}, showing its excellent cycling stability as cathode for high-performance PIHCs.

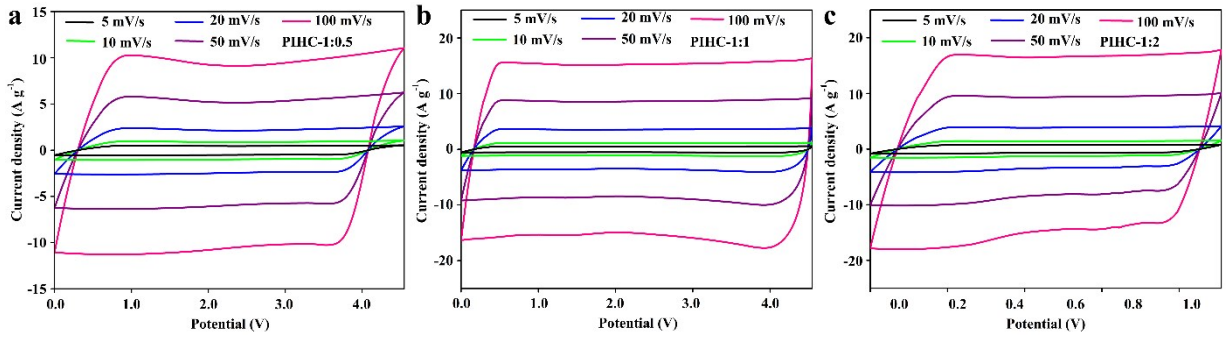

Figure S9. Typical CV curves of the CHTT-N//CHTT-N PIHCs at different scan rates of the 5-100 mV s^{-1} for the voltage window of 0-4.5 V.

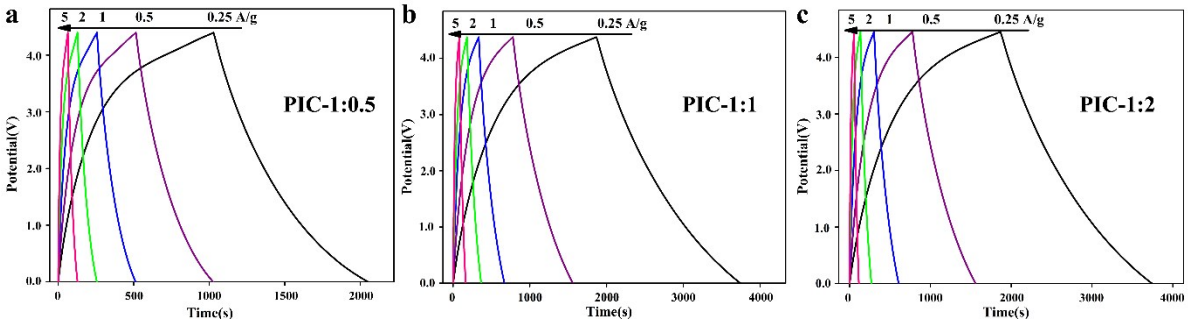

Figure S10. Typical charge-discharge curves of the CHTT-N//CHTT-N PIHCs at different current densities of the 0.25-5 A g^{-1} for the voltage window of 0-4.5 V.

Table S1 Comparison of the performances of CHTT-N and other high-performance carbon anodes from literatures.

Materials	Current density (mA g^{-1})	Capacity (mAh g^{-1})	Cycling Number (current density, mA g^{-1})	Ref.
NCNF-650	25	248	1000 (500)	1
NOHPHC	25	365	100 (50)	2
MoS_2@SnO_2@C	50	597	25 (50)	3
$MoSe_2$/N-Doped Carbon	100	300	300 (100)	4
PCM	50	230	200 (500)	5
CNS	100	252	1300 (2000)	6
S/N@C	50	320	900(2000)	7
V_2O_5@CNT Sponge	10	145	50(25)	8
Yolk-Shell FeS_2@C	1000	360	20(300)	9
Our work	100	397	3000(5000)	

References

1. Y. Xu, C. Zhang, M. Zhou, Q. Fu, C. Zhao, M. Wu, Y. Lei, *Nat. Commun*. **2018**, 9, 1720.
2. J. Yang, Z. Ju, Y. Jiang, Z. Xing, B. Xi, J. Feng, S. Xiong, *Adv. Mater*. **2018**, 30, 1700104.
3. Chen, Z.; Yin, D.; Zhang, M., *Small* **2018**, 14, 1703818.
4. Ge, J.; Fan, L.; Wang, J.; Zhang, Q.; Liu, Z.; Zhang, E.; Liu, Q.; Yu, X.; Lu, B., *Adv. Energy*

Mater. **2018**, 8,1801477.

5. M. Chen, W. Wang, X. Liang, S. Gong, J. Liu, Q. Wang, S. Guo, H. Yang, *Adv. Energy Mater*. **2018**, 8, 1800171.
6. J. Chen, B. Yang, H. Hou, H. Li, L. Liu, L. Zhang, X. Yan, *Adv. Energy Mater*. **2019**, 9, 1803894.
7. A. Mahmood, S. Li, Z. Ali, H. Tabassum, B. Zhu, Z. Liang, W. Meng, W. Aftab, W. Guo, H. Zhang, et al., *Adv. Mater*. **2018**, 30, 1805430.
8. Ye, F.; Lu, D.; Gui, X.; Wang, T.; Zhuang, X.; Luo, W.; Huang, Y., *J. Materiomics* **2018**, 2352-8478.
9. Zhao, Y.; Zhu, J.; Ong, S. J. H.; Yao, Q.; Shi, X.; Hou, K.; Xu, Z. J.; Guan, L., *Adv. Energy Mater*. **2018**, 8, 1802565.